Planet Detection Metrics:

Per-Target Detection Contours
for Data Release 25

NASA Ames Research Center
Moffett Field, CA 94035

Prepared by: _____ Date ___6/13/17___
Christopher J. Burke, Science Office

Prepared by: _____ Date ___6/13/17___
Joseph Catanzarite, Science Operations Center

Approved by: _____ Date ___6/13/17___
Michael R. Haas, Science Office Director
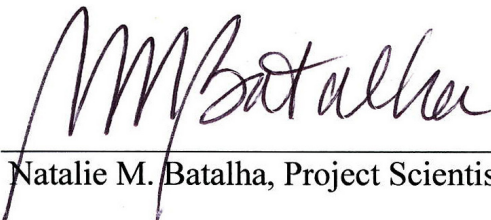
Approved by: _____ Date ___6/13/17___
Natalie M. Batalha, Project Scientist

Document Control

Ownership
This document is part of the Kepler Project Documentation that is controlled by the Kepler Project Office, NASA/Ames Research Center, Moffett Field, California.

Control Level
This document will be controlled under KPO @ Ames Configuration Management system. Changes to this document shall be controlled.

Physical Location
The physical location of this document will be in the KPO @ Ames Data Center.

Distribution Requests
To be placed on the distribution list for additional revisions of this document, please address your request to the Kepler Science Office:

> Michael R. Haas
> Kepler Science Office Director
> MS 244-30
> NASA Ames Research Center
> Moffett Field, CA 94035-1000
> Michael.R.Haas@nasa.gov

The correct citation for this document is: Burke, C. J. & Catanzarite, J. 2017, *Planet Detection Metrics: Per-Target Detection Contours for Data Release 25*, KSCI-19111-002

DOCUMENT CHANGE LOG

DATE	RELEASE	PAGES	CHANGES/NOTES
June 5, 2017	001	all	Original release
June 13, 2017	002	7	Changed number of targets in KSOC-5006 run

Contents

1   Introduction

A necessary input to planet occurrence calculations is an accurate model for the pipeline completeness (Burke et al., 2015). This document describes the use of the *Kepler* planet occurrence rate products in order to calculate a per-target detection contour for the measured Data Release 25 (DR25) pipeline performance. A per-target detection contour measures for a given combination of orbital period, $P_{\rm orb}$, and planet radius, $R_{\rm p}$, what fraction of transit signals are recoverable by the *Kepler* pipeline (Twicken et al., 2016; Jenkins et al., 2017). The steps for calculating a detection contour follow the procedure outlined in Burke et al. (2015), but have been updated to provide improved accuracy enabled by the substantially larger database of transit injection and recovery tests that were performed on the final version (i.e., SOC 9.3) of the *Kepler* pipeline (Christiansen, 2017; Burke & Catanzarite, 2017a). In the following sections, we describe the main inputs to the per-target detection contour and provide a worked example of the python software released with this document (Kepler Planet Occurrence Rate Tools – KeplerPORTs)[1] that illustrates the generation of a detection contour in practice. As background material for this document and its nomenclature, we recommend the reader be familiar with the previous method of calculating a detection contour (Section 2 of Burke et al., 2015), input parameters relevant for describing the data quantity and quality of *Kepler* targets (Burke & Catanzarite, 2017b), and the extensive new transit injection and recovery tests of the *Kepler* pipeline (Christiansen et al., 2016; Burke & Catanzarite, 2017a; Christiansen, 2017).

2   Planet Radius to Multiple Event Statistic

This section describes the calculation necessary to estimate the primary detection statistic employed in the Transiting Planet Search (TPS) algorithm, Multiple Event Statistic (MES) (Jenkins, 2002; Christiansen et al., 2012), at a point ($P_{\rm orb}$ and $R_{\rm p}$) of the detection contour. This is the first step toward calculating a detection contour, as we must estimate what the MES would be for a hypothetical planet for any given $P_{\rm orb}$ and $R_{\rm p}$ in the domain of the detection contour tailored for the stellar properties of the *Kepler* target. We employ this MES estimate to obtain a completeness estimate based upon the detection efficiency model which is expressed in terms of MES (see Section 3). To first order, the MES is proportional to and has the same dependence as the basic equation for transit signal-to-noise ratio,

$$SNR = \frac{\Delta}{\sigma}\sqrt{N_{\rm tran}}, \tag{1}$$

where Δ is the transit depth, σ is an estimate of the flux time series noise on a time scale equivalent to the transit duration, and $N_{\rm tran}$ is the number of transit events contributing to the detection. However, for sufficient accuracy for use in modeling the *Kepler* pipeline completeness, MES formally depends on how well the search template matches the transit signal and the time-varying noise estimate measured in TPS (the so-called Combined Differential Photometric

---

[1]https://github.com/nasa/KeplerPORTs

Precision (CDPP) time series, Christiansen et al., 2012; Thompson, 2016). For DR25, the MES estimate is given by,

$$MES_{\text{est}}(R_{\text{p}}, P_{\text{orb}}) = \frac{\Delta_{b=0}(R_{\text{p}}, \bar{\theta}_\star)}{\sigma_{\text{one}}(R_{\text{p}}, P_{\text{orb}}, \bar{\theta}_\star)} MES_{\text{cor}}, \tag{2}$$

where $\Delta_{b=0}$ is the transit depth for an impact parameter, $b = 0$, planet crossing, $\bar{\theta}_\star$ is a list of the stellar parameters ($R_\star$, $\log g$, and T_{eff}) of the target along with limb darkening parameters, σ_{one} is the one-sigma depth (OSD) function, and MES_{cor} is a scale factor (see below) to achieve agreement with the MES values calculated by TPS.

We employ $\Delta_{b=0}$ because it represents the maximum MES_{est} possible (for a given R_{p} and P_{orb}), there is a simple algebraic expression for the case of a limb darkened transit (Mandel & Agol, 2002, see case 10), and it provides a convenient reference point in order to take into account the distribution of MES values encountered for a given R_{p} and P_{orb} (see Section 4) in the detection contour modeling. Limb darkening parameters consistent with stellar parameters from the DR25 Stellar Catalog (Mathur et al., 2017) are provided in the DR25 *Kepler* Stellar Table for all *Kepler* targets searched for planets. The KeplerPORTs software provides a python implementation for calculating $\Delta_{b=0}$ modeled after Mandel & Agol (2002). The OSD function is described in Burke & Catanzarite (2017b). To summarize, the OSD function quantifies the transit signal depth that results in a MES=1 signal for a given transit duration, τ, and P_{orb}. At fixed P_{orb}, the one-sigma depth function takes into account effects such as the time varying CDPP noise, cadences deweighted during the search, and number of transit events while averaging these quantities over orbital phase. The OSD function depends on $\bar{\theta}_\star$ through predicting the expected τ at a given point in the detection contour. The OSD function values are tabulated over a very fine grid of P_{orb}, and the fourteen standard transit durations employed in the planet search in TPS (i.e., 1.5, 2.0, 2.5, 3.0, 3.5, 4.5, 5.0, 6.0, 7.5, 9.0, 10.5, 12.0, 12.5, 15.0 hr). KeplerPORTs provides python functions to compute τ for a given $\bar{\theta}_\star$, P_{orb}, and R_{p}, as well as code for interpolating the OSD function in order to implement Equation 2.

We verify the R_{p} to MES model by comparing MES_{est} from Equation 2 to the expected MES (MES_{exp}) as measured in the flux-level transit injection (FLTI) tests (Burke & Catanzarite, 2017a). The MES_{exp} as provided by the FLTI tests are calculated with the TPS algorithm itself, thus the FLTI MES_{exp} is the standard we are trying to match with the approach taken in Equation 2. For the MES comparison, we selected a subsample of 7199 targets from the available 32316 targets in the FLTI run having KSOC-5006 as its identifier (Burke & Catanzarite, 2017a). From these 7199 targets, 5742, remained after selecting a set of 'well-behaved' targets for the MES comparison (see Section 3 for a more detailed definition of 'well-behaved'). We dropped from consideration targets with >10% of cadences removed by the multiple planet search. Furthermore, we selected transit injections that have $b < 0.05$, transit duration <15 hours, pass the window function criteria with sufficient N_{tran} (Burke & Catanzarite, 2017b), and have $4.0 < MES_{\text{exp}} < 100.0$. If a target has at least 20 transit injection trials meeting the above criteria, we calculate the median ratio of $MES_{\text{ratio}} = MES_{\text{est}}/MES_{\text{exp}}$ for that target, assuming $MES_{\text{cor}} = 1$. Figure 1 shows the resulting MES_{ratio} as a function of target $R_\star$. The median MES ratio, $MES_{\text{cor}} = 1.003$, and the standard deviation around the median, $\sigma = 0.01$. Our simplified MES$_{\text{est}}$ calculation agrees well with the MES values provided by the TPS algorithm,

however, in order to improve the agreement, we apply the MES_{cor} correction factor when calculating MES_{est} for the detection contour model using Equation 2. Repeating the analysis on other subsamples of targets from the KSOC-5006 FLTI run yielded the same result.

As more thoroughly discussed in Section 3.6, the outliers in Figure 1 are correlated with parameters associated with suppressed recovery of transit signals in the *Kepler* pipeline. The full database of FLTI results can be employed to develop a higher order R_{p} to MES model and provide more accurate results for the outliers shown in the right panel of Figure 1. These higher order effects are an insignificant contribution to planet occurrence for the *Kepler* dwarf star target sample. We do not address them with the current R_{p} to MES model. Science efforts that require understanding *Kepler* pipeline completeness for individual targets, especially for targets with less well-behaved flux time series properties, may need to provide a higher fidelity R_{p} to MES model.
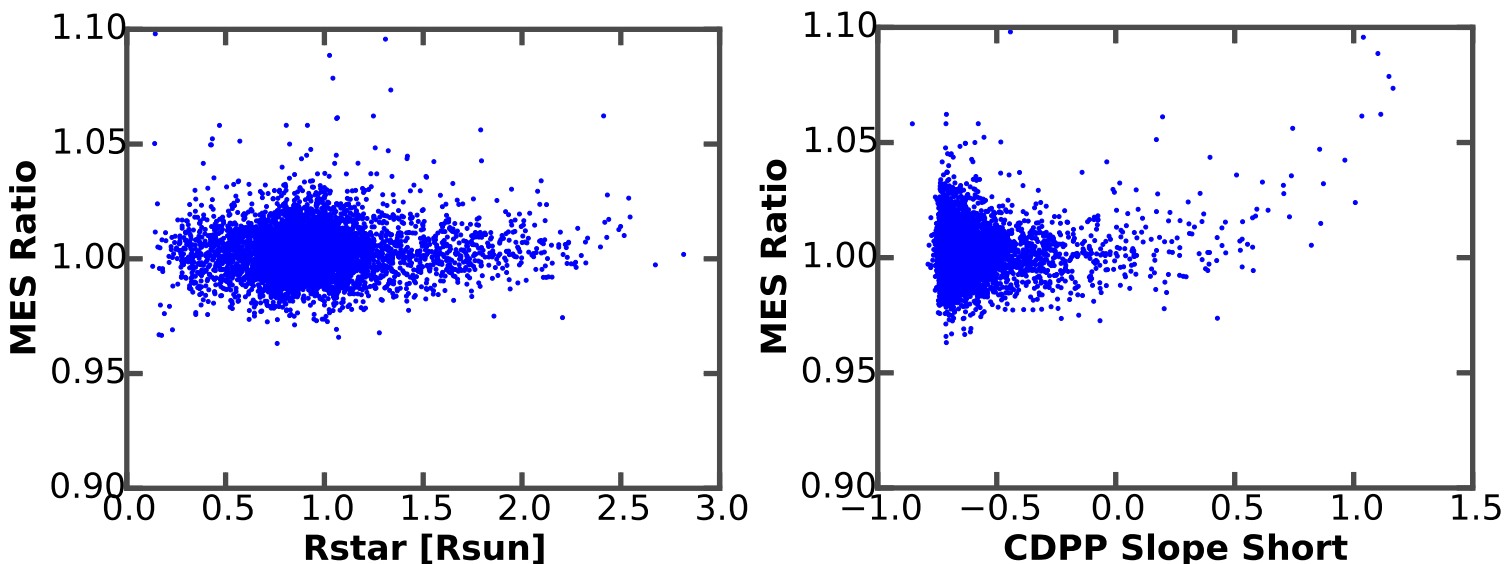
Figure 1: MES ratio between the MES estimated by Equation 2 assuming $MES_{\text{cor}} = 1$ and the MES as measured using the TPS algorithm as a function of $R_{\star}$(left panel) and as a function of CDPP slope (see Section 3.1) for short transit durations.

3 Per-Target Detection Efficiency Model

From previous analysis of the pixel level transit injection (PLTI) studies, Christiansen et al. (2016) noted that the average detection efficiency (DE) performance varied with varying selections of the target sample. A major emphasis of the DR25 analysis was to quantify this target-to-target variation of the DE. To support this effort, we performed a series of flux-level transit injection (FLTI) tests and released a database of 121 million transit injection and recovery tests that probe the behavior of the TPS module of the *Kepler* pipeline (Burke & Catanzarite, 2017a). Burke & Catanzarite (2017a) describe the FLTI output and illustrate the

generation of a DE curve for an individual target. The FLTI tests consist of a set of 'deep' FLTI runs with $\sim 10^5$ injections for a representative set of ~ 100 targets supplemented by 'shallow' FLTI runs with $\sim 10^3$ injections on a much larger set of $\sim 10^4$ targets. The deep and shallow runs complement each other for the development and validation of the per-target DE model and they help identify external variables that correlate with variations in the DE. The DE is a critical input for the detection contour, and previous planet occurrence rate calculations (Burke et al., 2015) employed the average DE derived from PLTI studies (Christiansen et al., 2015). The average DE derived from the PLTI study is still valid for occurrence rates, especially those involving large samples of targets. However, occurrence rate studies involving small subsets of *Kepler* targets should use the DE model described herein as it more accurately captures target-by-target variations.

3.1   Characterizing Stellar Noise Using CDPP Slope

Through trial and error, we determined that the external parameters that correlate most strongly with the empirical per-target DE variations measured from the FLTI tests are stellar radius ($R_\star$), CDPP slope, and orbital period ($P_{\rm orb}$). CDPP slope values are new to DR25 occurrence rate products, and we introduce them in this section before describing the DE model. CDPP slope values are tabulated for all targets as part of the DR25 *Kepler* Stellar Table (Burke & Catanzarite, 2017b). In order to calculate CDPP slope values, we begin with rmsCDPP values for the fourteen transit durations employed in the search by the TPS algorithm (Thompson, 2016). Under the assumption of white Gaussian noise in the flux time series, the rmsCDPP values decrease toward longer transit durations roughly as square root of the number of cadences in-transit. We quantify how well a target follows this expectation of white Gaussian noise by measuring the slope of rmsCDPP as a function of transit duration; a negative CDPP slope indicates that the flux time series satisfies the white Gaussian noise assumption. To capture the behavior in rmsCDPP trends with transit duration exhibited by *Kepler* targets, we calculate a CDPP slope for the short transit durations ($2 < \tau < 4.5$ hr), slpCDPP$_{\rm s}$, and long transit durations ($7.5 < \tau < 15$ hr), slpCDPP$_{\rm l}$. Figure 2 shows a scatter plot of CDPP slope (short versus long) for the targets studied as part of the FLTI test. Targets in the lower left corner of Figure 2 (negative CDPP slope values) empirically have a DE response closest to the theoretical expectation indicative of well-behaved flux time series data free of astrophysical noise. Targets that depart from the ideal white Gaussian noise properties have higher CDPP slope in both dimensions, and have suppressed DE curves. We define the lower left region of the CDPP slope plane (slpCDPP$_{\rm l} < -0.1$ and slpCDPP$_{\rm s} < -0.4$) as having well-behaved noise properties because the corrections for a suppressed DE inside this region are smaller than 5%. A majority (85%) of *Kepler* dwarf ($R_\star < 1.1\ R_\odot$) targets are in the well-behaved region of the CDPP slope plane and have the highest sensitivity DE curves.

Qualitatively targets with short, hourly time scale astrophysical variability populate the lower diagonal population that branches off from the densely populated area at slpCDPP$_{\rm l} = -0.4$ in Figure 2. Subgiants and giants generally populate the region toward higher slpCDPP$_{\rm l}$ and the upper right corner of the CDPP slope plane. It may be fruitful to investigate whether the information in the CDPP slope plane can be employed as a stellar gravity indicator in
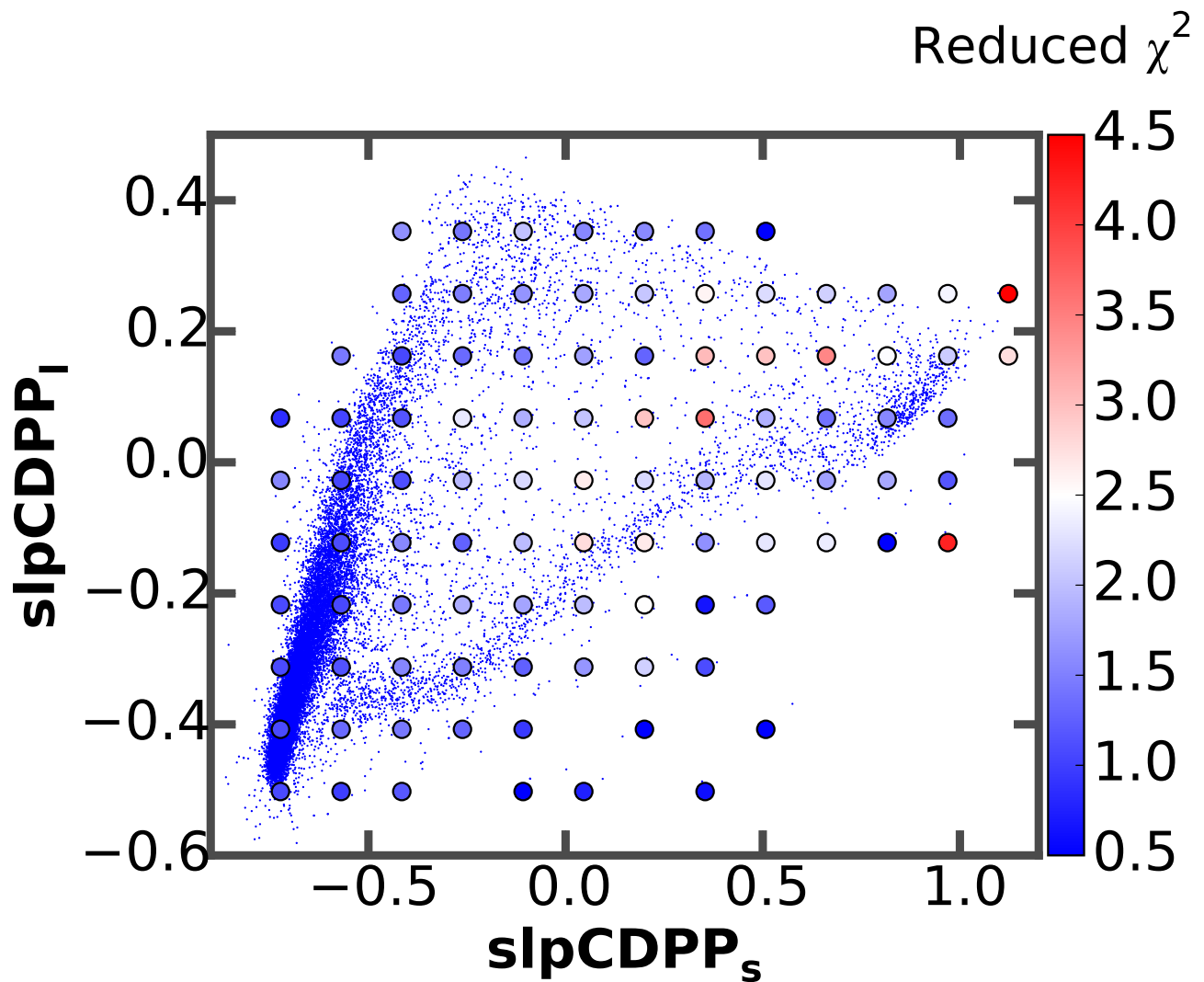
Figure 2: Distribution of the *Kepler* target noise properties in terms of slpCDPP$_s$ versus slpCDPP$_l$ (small points) for the subsample of targets with FLTI results. For purposes of modeling the DE, this CDPP slope plane is parceled into bins (large points represent bin centers) and corrections to the DE model are applied at these bin locations. The shading of the large points represents the reduced χ^2 between the final DE model and empirical DE measurements from the FLTI tests. The reduced χ^2 calculation is described in the text, but locations in the CDPP slope plane with a white to red color shading are locations where locally more than 10% of the targets have empirical DE that significantly disagree with the final DE model.

similar fashion to the 'flicker' noise metric of Bastien et al. (2016). Only targets chosen for the FLTI tests are shown. A subsample of these targets were selected to populate the CDPP slope plane uniformly, while others were selected randomly. Thus, the relative number of objects in Figure 2 in various regions is not representative of the full *Kepler* target sample.

3.2   Stellar Radius Detection Efficiency Dependence

The per-target DE model begins with a tabulation of the $R_\star$ dependence. In order to capture the average $R_\star$ dependence of the DE curve independent of other effects, we select targets from the shallow-run FLTI tests (FLTI run identifiers KSOC-5006 and KSOC-5104, Burke & Catanzarite, 2017a) that are in the well-behaved region of the CDPP slope plane. After quality cuts, 19099 targets had sufficient injections for inclusion in the analysis. In bins of 0.1 $R_\odot$, we calculate the median DE value as a function of MES within bins of ΔMES=1. We refer to these stellar radius dependent DE curves as the 'base DE' model, and they are shown in Figure 3 for select stellar radius bins. On average, the detection efficiency is suppressed for smaller stars (which, in this case, are the late type dwarf targets). This suppressed recovery derives predominately from the mismatch between the limb darkening profile for cool stars and the astrophysical template for transiting planets, which was designed to match the G dwarf targets in the *Kepler* sample (Seader et al., 2015). The tabulated base DE model is included as part of the KeplerPORTs software release as the file detectEffData_alpha_base_02272017.txt in ASCII format. The columns of the file are as follows: MES bin center, $R_\star$ bin center, DE value. The KeplerPORTs software provides python code for reading and implementing the base DE model.
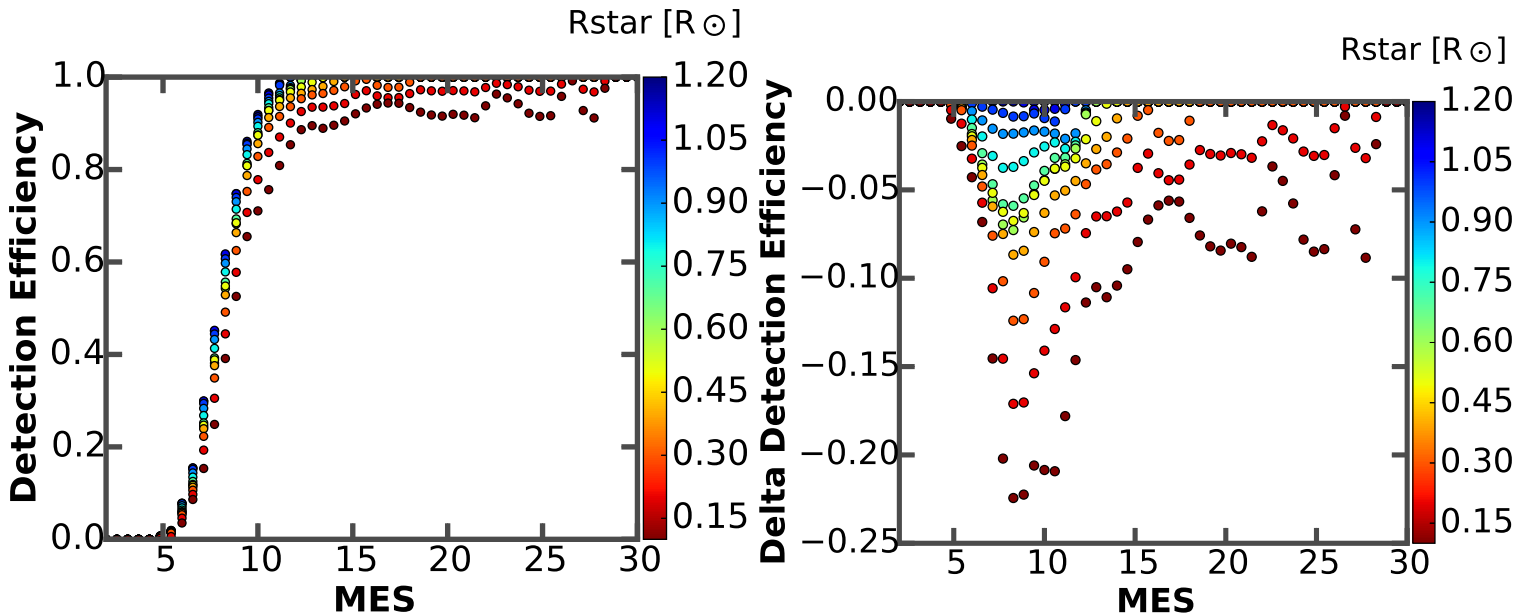
Figure 3: Base DE dependence on stellar radius according to the color shading (left panel) and the same data, but relative to the $R_\star$=1.2 $R_\odot$ DE (right panel).

3.3 CDPP Slope Detection Efficiency Model Correction

The next step is to extend the applicability of the base DE model beyond the well-behaved CDPP slope region. We determine a correction table to the base DE model on a grid across the CDPP slope plane shown in Figure 2. DE curves from the same shallow FLTI run as before (i.e., KSOC-5006, 5104) are examined, but now targets for the full CDPP slope plane are included. To determine the correction, we first compute the base DE model for each FLTI target by interpolating the grid of base DE model curves calculated in Section 3.2 using the appropriate $R_\star$ for each target. Then the difference between the base DE model and the empirically measured FLTI DE curve is calculated for all targets. The median of the base and empirical DE differences is measured in bins over the two dimensional CDPP slope plane. The large circles in Figure 2 show the bin centers over which the CDPP slope plane is parceled for determining the median DE offset. The DE offset is further parceled along the MES direction in bins of ΔMES=1, thus effectively making the CDPP slope plane DE correction into a three dimensional correction table. The tabulated CDPP slope plane DE model corrections are included as part of the KeplerPORTs software release as the file detectEffData_alpha12_SlopeLongShort_02272017.txt in ASCII format. The columns of the file are as follows: MES bin center, slpCDPP$_l$ bin center, slpCDPP$_s$ bin center, DE correction value. The KeplerPORTs software provides python code for reading and implementing the CDPP slope DE model corrections.

Figure 4 shows the CDPP slope plane DE correction as a function of MES for two values of slpCDPP$_l$ and lines of slpCDPP$_s$ given by the color shading. The left panel shows results for slpCDPP$_l = -0.34$, and the right panel shows results for slpCDPP$_l = 0.19$. The DE corrections in the CDPP slope plane indicate that targets with enhanced red noise present in the flux time series (high CDPP slope values) have reduced sensitivity for recovering planet signals. The DE curve represents the combined response of the vetoes implemented in the TPS algorithm (Twicken et al., 2016). The mechanisms responsible for the vetoes having similar DE response for targets with similar CDPP slopes are not fully understood, but the CDPP slopes empirically explain the DE variations observed in *Kepler* targets.

3.4 Orbital Period Detection Efficiency Model Dependence

The final step for the DE model accounts for dependence on $P_{\rm orb}$. There are not enough injections performed on each shallow FLTI target to quantify the period dependence. Thus, we employ the deep-run FLTI targets ($\sim$600,000 injections per target as described in Burke & Catanzarite, 2017a). We investigate the detection efficiency in five period bins bounded by 10, 60, 100, 200, 400, and 700 days. For each deep FLTI target, we calculate five empirical DE curves, one for each period bin. We also compute the base DE model for each target from Section 3.2. Both the empirical DE curve and the base DE model use a MES bin resolution of ΔMES=0.33. The base DE model is subtracted from the five period dependent empirical DE curves, yielding the residual DE offsets for the five period bins. We model the residual DE offset in each period bin independently using a linear function of the form,

$$\mathrm{DE_{resid}} = c_0 + c_1 \times N_{tr} + c_2 \times (\mathrm{CDPPSlopePlaneCorrection}), \qquad (3)$$
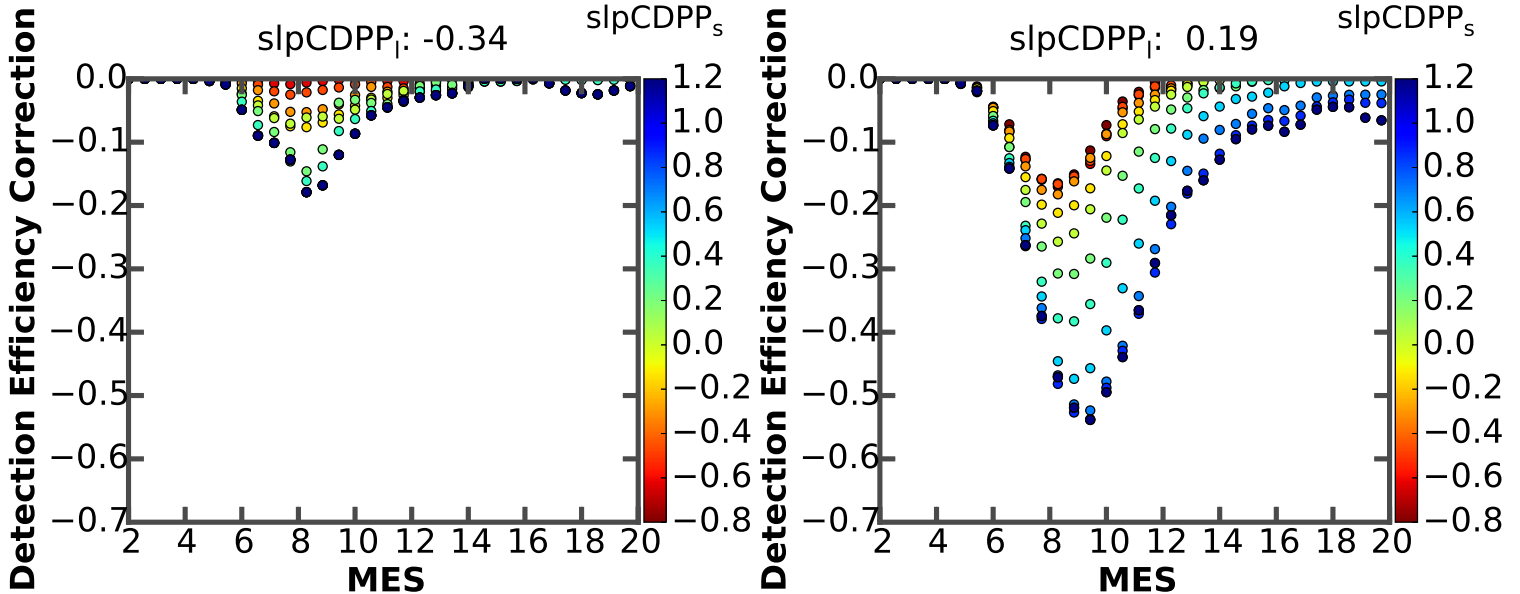
Figure 4: Corrections to the DE for fixed $slpCDPP_l = -0.34$ (left panel) and $slpCDPP_l = 0.19$ (right panel) for curves of increasing $slpCDPP_s$ from red to blue shading.

where N_{tr} is the expected number of transits at the midpoint of the period range (which depends on the data span and duty cycle for the star in question) and (CDPP Slope Plane Correction) is the interpolated correction determined in Section 3.3. In this linear model, we assume that the 'shape'/features of the CDPP slope plane correction does not depend on period other than a scaling factor, c_2. For each of the five period ranges and each MES bin, the coefficients that minimized the difference between the measured residual offset and the linear model are computed.

Not all three terms are warranted over the full (P_{orb}, MES) space. This is especially true where the DE is close to zero or unity. The constant, c_0, is used over the full parameter range. For MES<4.25 and MES>13.25 in the shortest period bin and for MES>20 in the longest period bin, both c_1 and c_2 are set to zero. The second term, c_1, is set to zero for all but the two shortest period bins. The third term, c_2, is set to zero when the absolute value of the CDPP slope plane correction (see Figure 4 for example corrections) interpolated to the MES bin center and target's CDPP slope values is less than 0.003 when averaged over targets. These coefficients are stored in the HDF5 format file detectEffData_alpha12_02272017.h5, and the KeplerPORTs software provides an example of their extraction and implementation for the per-target DE model.

3.5   Efficacy of the Per-target Detection Efficiency Model

Overall, the per-target DE model requires six inputs: $R_\star$, $slpCDPP_l$, $slpCDPP_s$, duty cycle, data span, and P_{orb}. The KeplerPORTs software provides an implementation in python that reads in the requisite data tables and the necessary interpolations to yield a DE curve for the

given set of inputs. Figure 5 shows the resulting DE model curves for the five period bins employed in the per-target DE model for a target in the well-behaved CDPP slope plane region (left panel) and for a target in the suppressed DE region of the CDPP slope plane (right panel). The DE is lower and has a stronger period dependence in the presence of red noise in the flux time series.
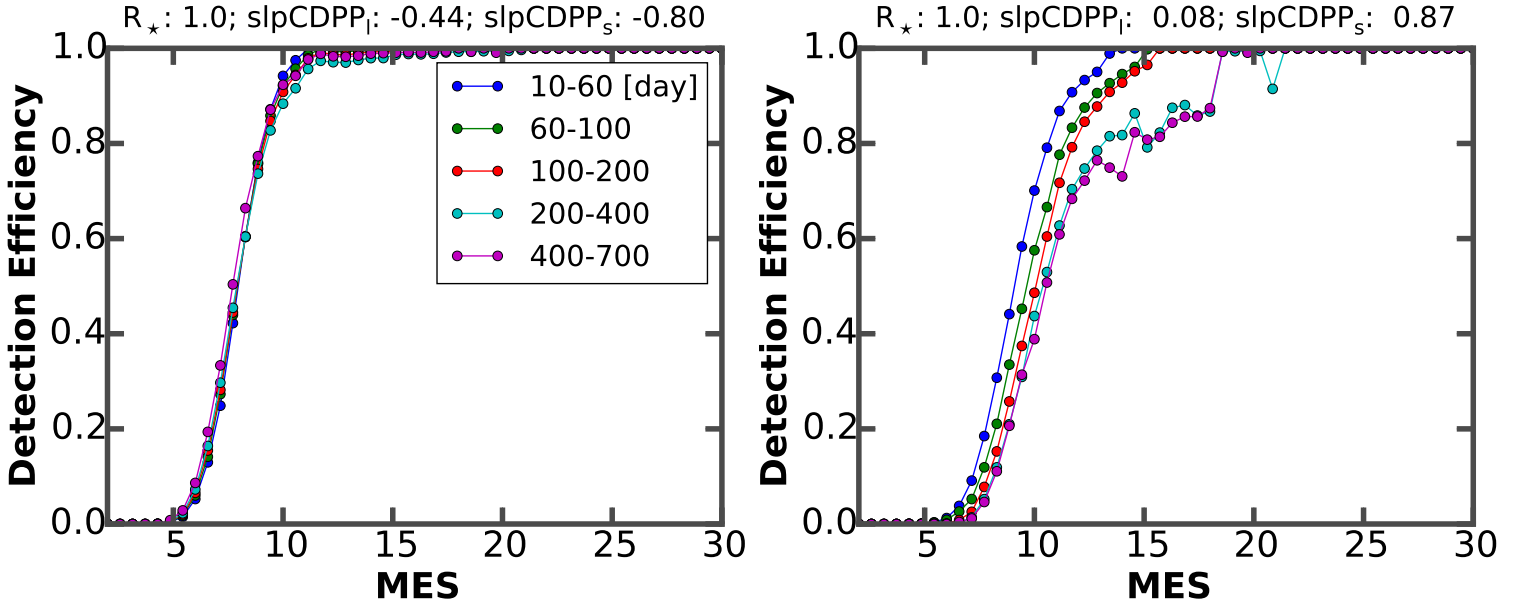
Figure 5: Example per-target DE model for the five period bins (i.e., blue, green, red, cyan, and magenta) with increasing $P_{\rm orb}$ for the well-behaved CDPP slope plane region (left panel) and for the upper right of the CDPP slope plane (right panel).

Figure 2 shows the quality of the per-target DE model for targets across the CDPP slope plane. The large points are color shaded by the reduced χ^2 between the DE model and empirical DE from the shallow-run FLTI targets. For a representative value of reduced χ^2 in each grid region of the CDPP slope plane, we adopt the upper $90^{\rm th}$ percentile of reduced χ^2 values. The reduced χ^2 is calculated in the transition region (5<MES<12) of the DE. In calculating the uncertainty in the empirical DE FLTI measurement for use in χ^2, we employ the analytic Bayesian parameter estimation model using a binomial model likelihood and an uninformative beta distribution ($\alpha = 0.5$, $\beta = 0.5$) prior. This idealized uncertainty model tends to under predict the per bin MES scatter, thus we remove the largest outlier before calculating reduced χ^2 resulting in seven degrees of freedom for the seven MES bins that contribute to the χ^2 calculation. A reduced $\chi^2 \sim 2.5$ with seven degrees of freedom represents a 3-σ residual from the model. Thus, locations in the CDPP slope plane with a white to red color shading are locations where locally more than 10% of the targets have empirical DE that significantly disagree with the DE model.

3.6   Limitations of the Per-target Detection Efficiency Model

The per-target DE model is not applicable to all *Kepler* targets. Several categories of targets strongly deviate from the model. First, the DE model is not applicable for targets with transit durations >15 hr, where FLTI tests reveal a strong suppression of transit signals. This occurred because the TPS algorithm was run with a maximum search transit duration of 15 hr, which also determined the time scale over which the whitening filter in TPS aims to protect transit signals. Thus, transit signals on time scales longer than 15 hr are removed by the whitening filter and FLTI tests show that transit signals with longer transit durations have highly suppressed DE curves. **The 15 hr limitation is suitable for accommodating dwarf star, $R_\star <$ 1.25 $R_\odot$ targets with modest eccentricities. However, researchers wanting to perform occurrence rate studies on subgiant and giant *Kepler* targets will need to explore the full database of FLTI information and derive a more complete DE model.** In solving for the current per-target DE model, all transit injections that resulted in a transit duration >15 hr were removed from consideration.

The second limitation is for targets which have significant amounts of in-transit data removed in subsequent searches for additional transiting planets. The *Kepler* occurrence rate data products are designed to quantify pipeline completeness under the assumption that the target is planet free. Thus, the input to FLTI tests and noise estimates for occurrence rate purposes are performed on a flux time series where transits identified in the DR25 pipeline run are effectively removed by replacement and fully deweighting the cadences so as not to contribute to the planet search or noise statistics. Examination of the FLTI results finds that targets with >10% of their data removed from previously identified transits have suppressed DE curves. The population of targets with >10% of data removed with $P_{\rm orb}$>10 days is small (5% of *Kepler* targets and 10% of *Kepler* targets with planet candidate KOIs). Thus it is safe to ignore this effect for planet occurrence rates $\gtrsim$ 10 days. However, for investigations of multi-planet systems with a short period ($P_{\rm orb}$<3 day) planet, the DE model is likely optimistic after cadences from the first identified planet are removed. In solving for the per-target DE model, we adopted a more conservative threshold and do not consider FLTI injections on targets that experienced >5% fractional decrease in the duty cycle from removal of planet signal cadences. The fractional duty cycle drop during the DR25 pipeline run can be obtained for all *Kepler* targets in the DR25 Stellar Table by comparing the tabulated values of the duty cycle calculated before and after the pipeline has identified all transit events (i.e., utilize the parameters "dutycycle" and "dutycycle_post" in Appendix A of Burke & Catanzarite (2017b)).

Finally, we examined targets that are not well-fit by the final DE model. We identify two characteristics of their flux time series that are common to the targets not well modeled. We do not attempt to model the impact on the DE using these additional characteristics. However, we qualitatively describe the behavior and provide a list of targets that are not well characterized by the per-target DE model. The first notable characteristic regards flux brightening events that occur on the transit timescale. In the presence of such features, the brightening systematic offsets/fills-in the dimming transit signal and prevents its recovery. We developed a metric that quantifies targets influenced by systematic brightening features. We employ diagnostic information from the TPS algorithm that provides an estimate of the depth of a purported

transit signal centered on every cadence. From the depth estimate time series, we formulate a metric that identifies targets with brightening systematics that cause a heavy tail in the distribution of depth estimates relative to the Gaussian distribution.

The second metric examines the properties of the wavelet based whitening filter employed in TPS. In the presence of strong astrophysical noise, the whitening filter can have a higher amplitude of signal suppression and be more aggressive at detrending the data. The more aggressive the whitening filter, the greater the tendency for transforming a u-shaped transit signal into a signal concentrated exclusively at the ingress and egress cadences and suppressing the transit depth. We developed a metric that quantifies this shape change, as anecdotal evidence shows that when the filtered transit signal shape is concentrated into a small number of ingress and egress cadences, the veto algorithms in TPS are more susceptible to stochastic and systematic variations of single cadences. Both these metrics are calculated on the flux time series data after planet signals have been removed by the planet search. The external file, DR25_DEModel_NoisyTargetList.txt, lists the Kepler ID for 8629 targets that have elevated values of these two metrics and empirically are outliers from the DE model. This list contains 1.2% of the GKM *Kepler* dwarf star targets.

In summary, the per-target DE model should not be used for targets with $R_\star > 1.25\ R_\odot$, targets with an expected transit duration >15 hr, multi-planet systems with fractional duty cycle drops >10%, and the targets reported to have deviant flux time-series (i.e., see DR25_DEModel_NoisyTargetList.txt).

4   MES Smearing

The next stage of calculating a detection contour involves mapping the MES estimate of a hypothetical planet with a given P_{orb} and R_p (Section 2) to a recovery fraction via the DE model. Section 3 describes a per-target DE model new to DR25 that characterizes the recovery fraction as a function of MES. One can also adopt the target averaged DE model based upon the PLTI test (Christiansen, 2017). However, before employing any DE model for a detection contour calculation, one additional conditioning step is necessary to achieve agreement between the FLTI tests (Burke & Catanzarite, 2017a) and the detection contour models described in Burke et al. (2015). The model deficiency occurs in the process of converting MES to detection probability using the DE model alone. A more accurate conditioning of the DE model is needed that properly takes into account the distribution of impact parameters which we call the 'MES smearing effect'. Specifically, for a given point $[P_{orb}, R_p]$ in the detection contour, the impact parameter acts as a third dimension which influences the recoverability of a transit signal. MES smearing is a method to properly marginalize over the third dimension of impact parameter for transit signal recoverability when modeling a detection contour, rather than the previous method of treating the impact parameter distribution inaccurately with a point estimate.

For a given R_p, MES is maximum for impact parameter, b=0, but MES decays toward zero for higher impact parameters due to limb darkening effects and eventually due to grazing geometry. The previous procedure for estimating the recovery fraction at the average impact parameter is inaccurate, since this point estimate of the detection probability does not take

into account the asymmetric high impact parameter tail towards low MES. The left panel of Figure 6 shows an example target where we have plotted the MES as a function of impact parameter over a small region of $P_{\rm orb}$ and $R_{\rm p}$ from the FLTI output. The MES in Figure 6 has been normalized to the median MES for impact parameters near zero ($b < 0.05$). The right panel of Figure 6 shows data similar to the left panel, but displayed as a histogram of the normalized MES values built from the average of 50 trial [$P_{\rm orb}$, $R_{\rm p}$] locations (blue points). We find that MES as a function of impact parameter does not vary with $P_{\rm orb}$ or $R_{\rm p}$ for a given target. The normalized MES distribution varies between zero and one, thus a beta distribution probability describes the MES distribution well. The green line shows a beta distribution fit to the empirical MES distribution. The sudden drop off at MES<0.2 is an artifact of only injecting transits with $b < 1$ rather than injecting up to the full grazing transit with $b = 1+R_{\rm p}/R_{\star}$.
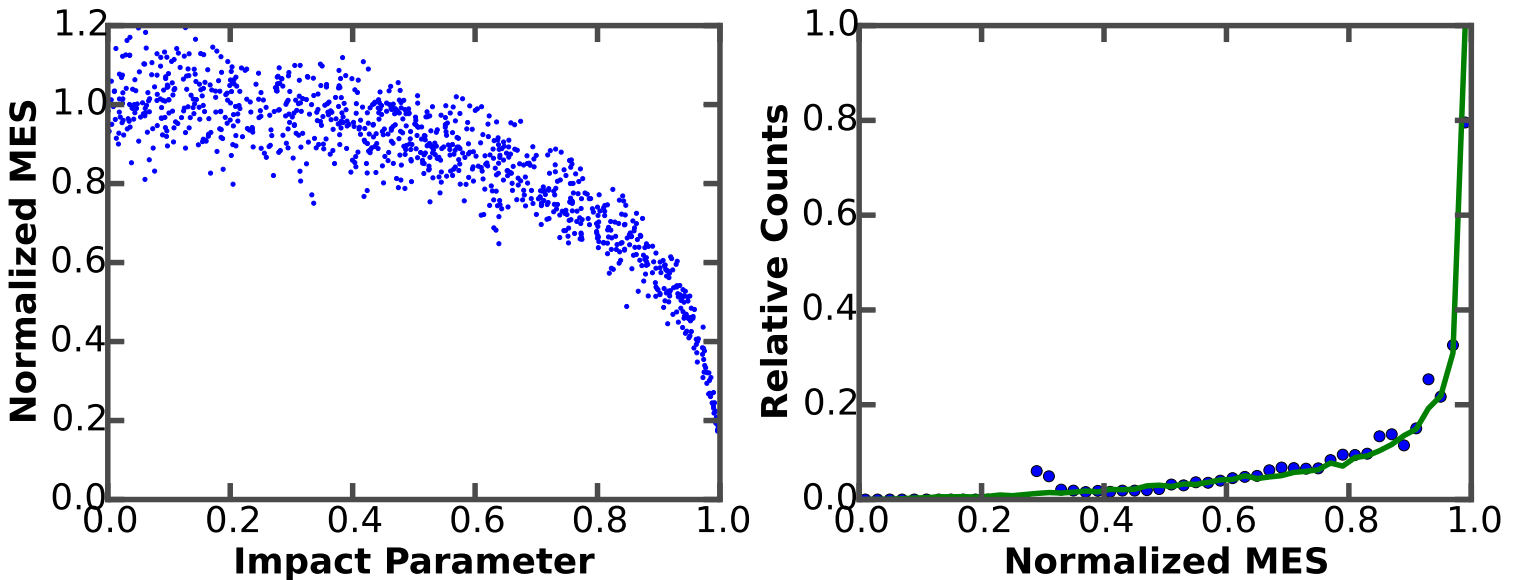
Figure 6: Scaled MES as a function of impact parameter for a small region of $P_{\rm orb}$ and $R_{\rm p}$ from the FLTI output (left panel). Resulting distribution of MES values built from 50 trial ($P_{\rm orb}$, $R_{\rm p}$) locations (blue points) and a beta distribution fit to the MES distribution (green line).

In practice, MES smearing is applied to the DE model from Section 3 using a Monte-Carlo integration method. The effective, smeared DE calculation is performed for every MES bin of the original DE model. In this MES smeared representation of the DE model, the MES of the bin represents the highest MES, $b = 0$, transit signal. MES smearing is calculated by sampling from the beta probability distribution and converting the beta distribution samples, which range from 0-1 into MES scaled by the current MES bin value. The beta-distributed scaled MES values are converted to recovery fractions from the original DE curve. The resulting recovery fraction sample is averaged to provide the final 'smeared' DE curve. Figure 7 shows a model DE from Section 3 (dash line) and the same model after applying the MES smearing distribution (solid line).

We have found from FLTI tests that the MES distribution as a function of impact parameter

is not the same for all targets. For targets with higher levels of astrophysical variability, and/or red noise, the whitening filter in TPS is more aggressive and the MES distribution with impact parameter is flatter. Empirically, we find that the slpCDPP$_l$ is a good proxy to identify targets with flattened MES distributions. When modeling the MES distribution for the FLTI targets, we find a quadratic function in slpCDPP$_l$ describes the beta distribution parameters.

$$a = 5.324687 \times CSL^2 + 3.622976 \times CSL + 2.753682 \tag{4}$$

$$b = -0.288250 \times CSL^2 - 0.118463 \times CSL + 0.450678, \tag{5}$$

where a and b are the two parameters of the beta distribution and CSL=slpCDPP$_l$. From the deep-run FLTI targets (FLTI run identifiers KSOC-5004, KSOC-5008, and KSOC-5125 from Burke & Catanzarite, 2017a), we fit the beta distribution parameters to a sample of 72 targets after quality control cuts. See the KeplerPORTs software for the implementation of MES smearing for building a detection contour.

5   Window Function

The window function specifies the fraction of phase space as a function of P_{orb} such that the minimum detection requirements (such as having at least three transit events) are met. See Burke & McCullough (2014); Burke et al. (2015); Burke & Catanzarite (2017b) for a description of the full details of the window function. Implementation of the window function in a detection contour has not changed since Burke et al. (2015) with the exception that a detailed numerical model of the *Kepler* window function is now available (Burke & Catanzarite, 2017b).

6   Detection Contour

Construction of a detection contour for *Kepler* pipeline completeness and its application for planet occurrence rate analysis is described in Burke et al. (2015). The DR25 detection contour model follows the general procedure of Burke et al. (2015), but updates the inputs for much improved accuracy and precision. The previous sections describe each of the steps for constructing a detection contour, and for the convenience of the end user, we are releasing the DR25 KeplerPORTs python module that provides code for all the steps discussed in this document and illustrates the calculation of a detection contour for a single target. The inputs to KeplerPORTs are the window function and one-sigma depth function data products available for download at the NASA Exoplanet Archive and documented in Burke & Catanzarite (2017b), data tables for the per-target detection efficiency model (released as standalone files with the KeplerPORTs software), and a set of input values ($R_\star$, slpCDPP$_l$, slpCDPP$_s$, duty cycle, data span, limb darkening coefficients) available from the DR25 *Kepler* stellar data table's occurrence rate columns (Burke & Catanzarite, 2017a,b).

As an example use of KeplerPORTs to generate a single target detection contour, Figure 8 shows the resulting detection contour for the target KIC 3429335. For comparison, we show an empirical detection contour derived from the FLTI test in Figure 9. The difference between
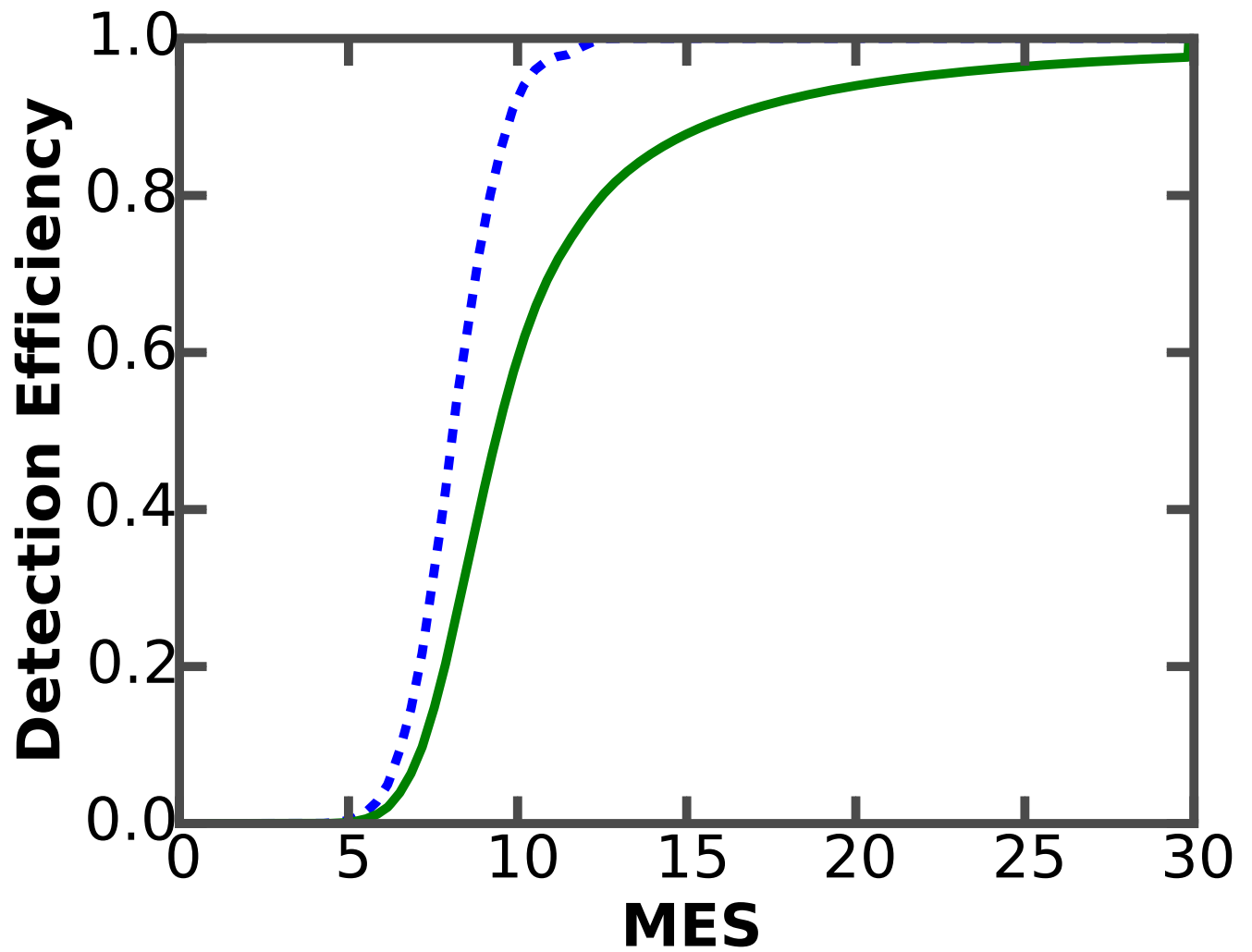
Figure 7: DE model curve from Section 3 (dash line) and after MES smearing has been applied (solid line) for the properties of KIC 8311864, host to Kepler-452b (Jenkins et al., 2015).

the model and empirical detection contour is shown in Figure 10, which demonstrates the good agreement between the two.

7   Epilogue

The detection contour model described in this document and implemented by the KeplerPORTs software only quantifies the recoverability of transiting planet signals due to the *Kepler* pipeline. In other words, it accurately portrays the ability of the *Kepler* pipeline to generate a Threshold Crossing Event (TCE) for a given hypothetical planet (Twicken et al., 2016; Jenkins et al., 2017). However, the subsequent classification steps that turn TCEs into *Kepler* Objects of Interest (KOI) and then disposition them (Coughlin et al., 2016, Thompson et al., in preparation) as planet candidates (PCs) or false positives (FPs) is not accounted for by these detection contours. Thus, for accurate planet occurrence rate calculations using the *Kepler* PC population, one must augment the detection contours for the completeness of these classification steps (Burke et al., 2015). The effective completeness of the classification steps can take the form of an additional DE curve that multiplies the per-target *Kepler* pipeline DE model of Section 3. The raw data to derive the classification DE curve is described in Coughlin (2017) and available through the NASA Exoplanet Archive. In addition to completeness, any detection experiment must quantify the potential for false alarms (or type I errors) contaminating the PC sample (referred to as planet sample reliability). In DR25, we introduced several tests that quantify the level of false alarm contamination (Coughlin, 2017, Thompson et al., in preparation). The completeness of the classification steps and planet sample reliability have not been included in any *Kepler* planet occurrence rate calculations to date. A major advancement for the final DR25 *Kepler* planet catalog is that planet occurrence rates can finally take into account these important contributions that ultimately shape the detected planet sample (Burke et al., 2015, Thompson et al., in preparation).
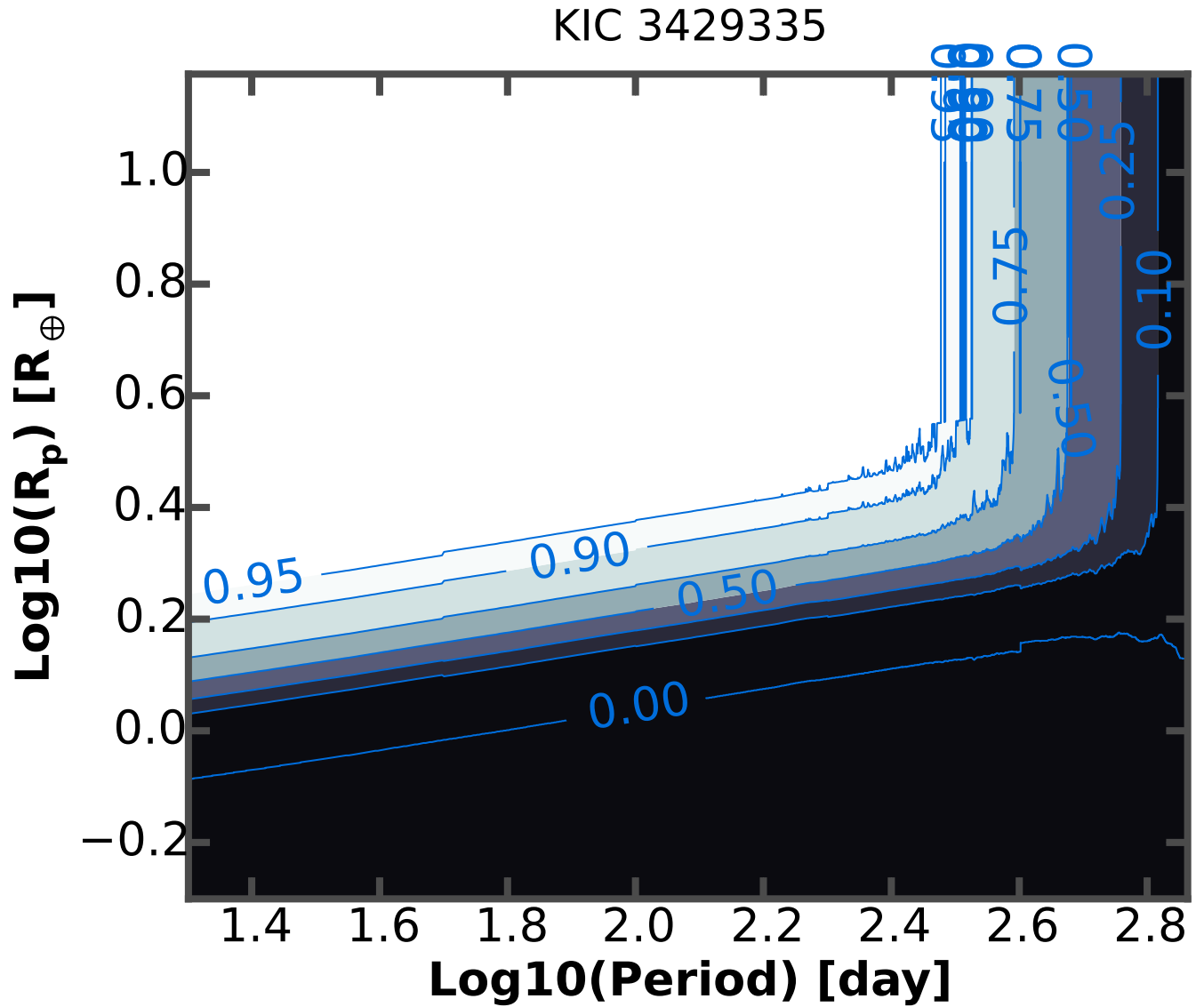
Figure 8: Detection contour model for KIC 3429335 using the KeplerPORTs software and the inputs described in this document.
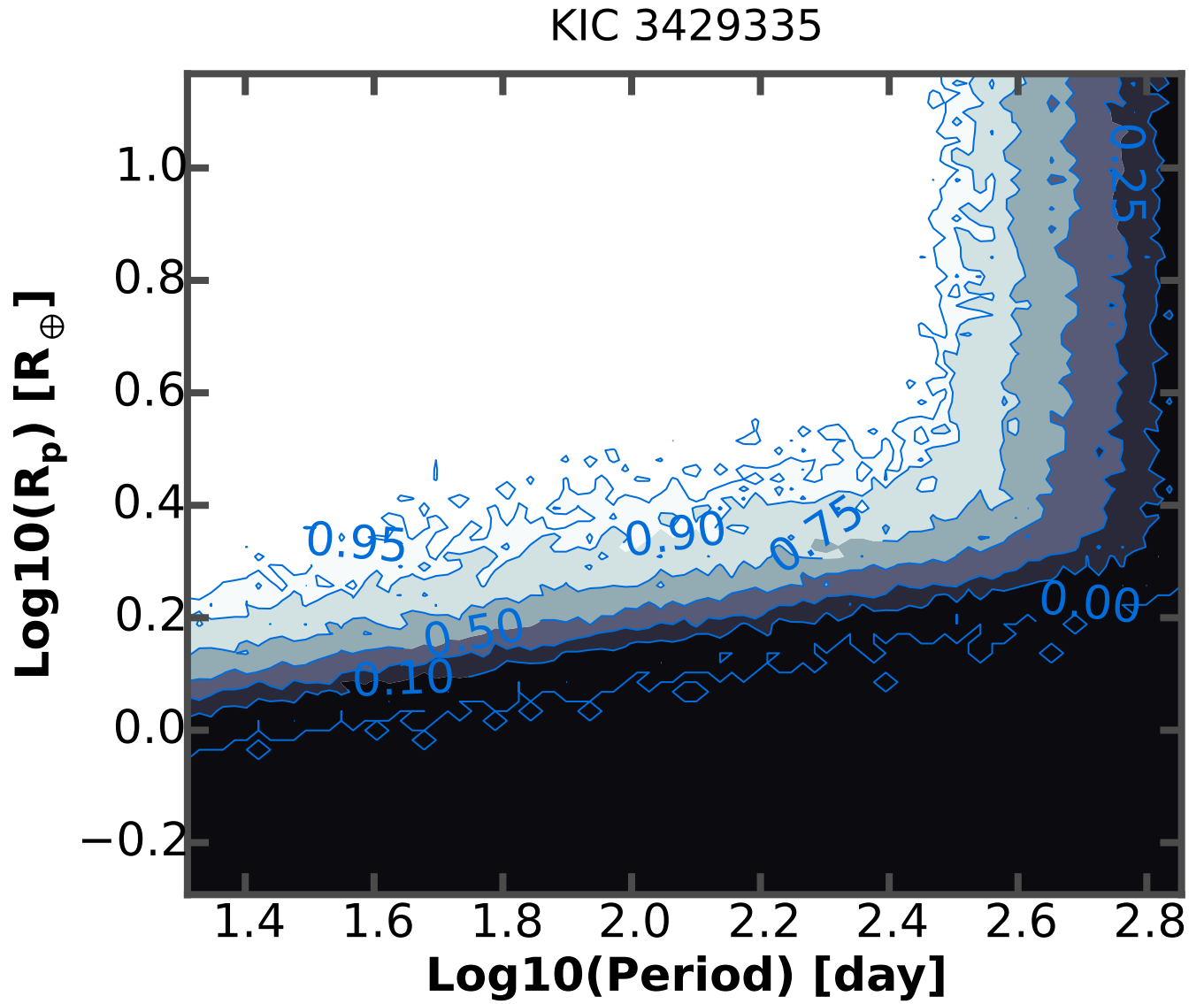
Figure 9: Empirical detection contour for KIC 3429335 using the FLTI output data set for this target.
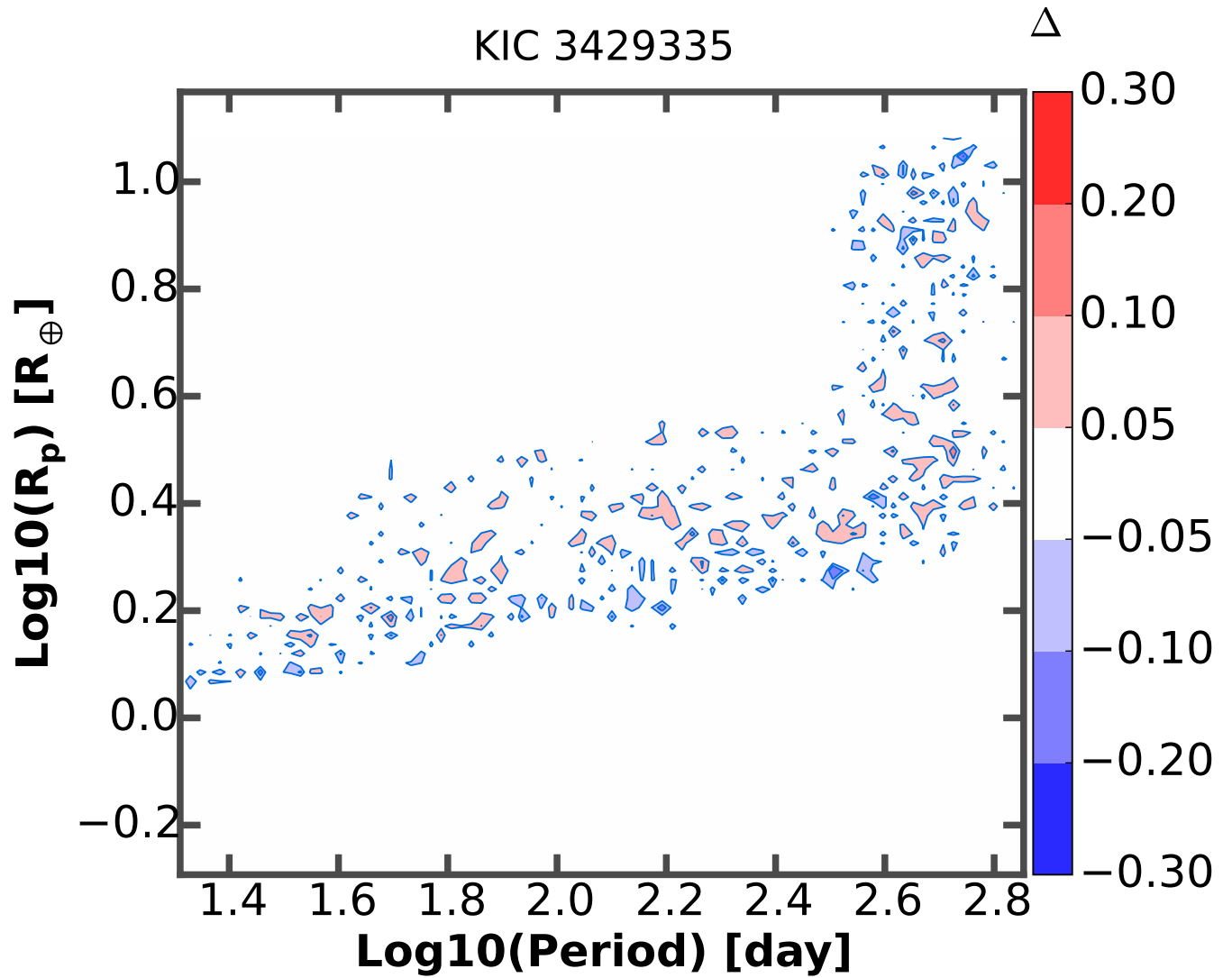
Figure 10: Difference between the detection contour model (Figure 8) and the empirical detection contour (Figure 9) for KIC 3429335.

References

Bastien, F. A., Stassun, K. G., Basri, G., & Pepper, J. 2016, ApJ, 818, 43

Burke, C. J., & McCullough, P. R. 2014, ApJ, 792, 79

Burke, C. J., Christiansen, J. L., Mullally, F., et al. 2015, ApJ, 809, 8

Burke, C. J., Catanzarite, J. 2017a, Planet Detection Metrics: Per-Target Flux-Level Transit Injection Tests of TPS for Data Release 25 (KSCI-19109-001)

Burke, C. J., Catanzarite, J. 2017b, Planet Detection Metrics: Window and One-Sigma Depth Functions for Data Release 25 (KSCI-19101-002)

Christiansen, J. L., Jenkins, J. M., Caldwell, D. A., et al. 2012, PASP, 124, 1279

Christiansen, J. L., Clarke, B. D., Burke, C. J., et al. 2015, ApJ, 810, 95

Christiansen, J. L., Clarke, B. D., Burke, C. J., et al. 2016, ApJ, 828, 99

Christiansen, J. L. 2017, Planet Detection Metrics: Pixel-Level Transit Injection Tests of Pipeline Detection Efficiency for Data Release 25 (KSCI-19110-001)

Coughlin, J. L., Mullally, F., Thompson, S. E., et al. 2016, ApJS, 224, 12

Coughlin, J. L. 2017, Planet Detection Metrics: Robovetter Completeness and Effectiveness for Data Release 25 (KSCI-19114-001)

Jenkins, J. M. 2002, ApJ, 575, 493

Jenkins, J. M., Twicken, J. D., Batalha, N. M., et al. 2015, AJ, 150, 56

Jenkins, J. M. 2017, *Kepler* Mission Data Processing Handbook (KSCI-19081-002)

Mandel, K., & Agol, E. 2002, ApJ, 580, L171

Mathur, S., Huber, D., Batalha, N. M., et al. 2017, ApJS, 229, 30

Seader, S., Jenkins, J. M., Tenenbaum, P., et al. 2015, ApJS, 217, 18

Thompson, S. E. 2016, Data Validation Time Series File: Description of the File Format and Content, KSCI-19079-001

Twicken, J. D., Jenkins, J. M., Seader, S. E., et al. 2016, AJ, 152, 158